A VESSEL KEYPOINT DETECTOR FOR JUNCTION CLASSIFICATION

Chetan L Srinidhi[1*]   *Priyadarshi Rath*[2*]   *Jayanthi Sivaswamy*[2]

[1] National Institute of Technology Karnataka, Surathkal, India

[2] Centre for Visual Information Technology, IIIT-Hyderabad, India

ABSTRACT

Retinal vessel keypoint detection and classification is a fundamental step in tracking the physiological changes that occur in the retina which is linked to various retinal and systemic diseases. In this paper, we propose a novel Vessel Keypoint Detector (VKD) which is derived from the projection of log-polar transformed binary patches around vessel points. VKD is used to design a two stage solution for junction detection and classification. In the first stage, the keypoints detected using VKD are refined using curvature orientation information to extract candidate junctions. True junctions from these candidates are identified in a supervised manner using a Random Forest classifier. In the next stage, a novel combination of local orientation and shape based features is extracted from the junction points and classified using a second Random Forest classifier. Evaluation results on five datasets show that the designed system is robust to changes in resolution and other variations across datasets, with average values of accuracy/sensitivity/specificity for junction detection being 0.78/0.79/0.75 and for junction classification being 0.87/0.85/0.88. Our system outperforms the state of the art method [1] by at least 11%, on the DRIVE and IOSTAR datasets. These results demonstrate the effectiveness of VKD for vessel analysis.

Index Terms— Retinal images, Keypoint detection, Vessel landmarks, Junction classification.

1. INTRODUCTION

Retinal vessel analysis is of interest to detect and assess diseases such as diabetes, hypertension, stroke, and arteriosclerosis which bring about structural and geometrical changes in retinal vasculature [2, 3]. Changes in vascular patterns at the vessel bifurcation and crossover points provide vital information for diagnosis of various systemic and cardiovascular diseases. Hence, an analysis of keypoints on a vessel tree is of interest. Detecting keypoints is challenging as junctions may appear close to each other, or at extremely low contrast regions. When vessels that appear parallel to each other change

---

⋆ Equal contribution authors

courses, they create a virtual bifurcation or crossover. More generally, the spatially varying nature of vessel calibre and density in an image poses a challenge to accurate detection of keypoints and their characterization.

Automatic detection of junctions, which are a specific type of keypoint has attracted much interest. Junction detection and classification have been attempted in the past using vessel maps or models. Skeletonization of vessel maps in [4, 5, 6, 1] is followed by analysis in a window around a vessel pixel to assess if the pixel is a keypoint such as bifurcation or crossover. Both circular [5] and square shaped windows [4] have been considered. Evidence gathering by pixel voting followed by a refinement based on distance between pixels is typically used to locate bifurcations and crossovers. In contrast, the model-based techniques employ shifted Gabor filters [7] or eigen analysis of Hessian at the vessel point [8]. More recently, orientation scores derived by correlating image patches with anisotropic wavelets [6, 1] have been proposed as a basis to detect junctions and subsequently classify them as bifurcations or crossovers. This approach was quite successful in modelling different kinds of complex junction locations. Existing approaches for detecting keypoints model the orientation of the vessel in a local neighborhood without explicitly considering the larger context or shape information which might aid in handling ambiguities. In our work, we propose a learning based approach that combines orientation and shape information for detecting and classifying keypoints. Our strategy is shown to be robust, accurate and reliable.

The major contributions of our work are the following: i) a novel vessel keypoint detector which is useful in detecting interest points on the vessel tree, ii) an end-to-end retinal vessel junction detection and classification system, and iii) a thorough validation on five publicly available retinal datasets. We next present the method and the experiments conducted along with the results obtained.

2. VESSEL KEYPOINT DETECTOR

One of the basic tasks in vessel tree analysis is identifying keypoints such as junctions, as they serve as landmarks useful in the registration of retinal images and in biometrics. Clin-

ically, vessel keypoints such as bifurcation points are of interest in assessing diseases such as retinopathy of prematurity via the branch angle at these points. Retinal vessels vary significantly in their size, shape, and orientation. Further, in detecting keypoints local as well contextual information is useful in resolving ambiguities and overcoming problems due to the variability in morphology and orientation.

We propose a novel Vessel Keypoint Detector (VKD) which is designed to operate on a binary vessel map and extract points of interest in the vessel tree. All vessel maps are skeletonized first to handle varying vessel calibre within and across images. Next, around every vessel point p, we consider a region of interest (ROI) $R_p(x, y)$ and apply a log-polar transform to obtain $R_p(r, \theta)$. The log mapping preserves information close to a vessel point while increasingly compressing the information as one moves away from the vessel point in a non-linear fashion. Fig. 1 shows sample ROI's with different vessel patterns of interest and the corresponding log-polar mapped results. The number of vertical lines depends on the pattern (straight vessel segment, crossing vessels, branching vessels etc.) and their position depends on the orientation of the vessels in $R_p(x, y)$.

We next do a vertical projection of $R_p(r, \theta)$ to obtain a vector $R_p(\theta)$. In order to build robustness to spurious vessels and varying vessel calibre, the range of r is limited to an interval $[R_1, R_2]$ where as $\theta \in [0°, 360°]$. Since r and θ have to be discrete variables (say m, n) we do so with sampling rates of Δ_r and Δ_θ. The obtained projection $R_p(\theta)$ provides a count of the number of pixels in a vessel fragment at a specific θ. This is binarized with a threshold set at 1 to obtain a vessel keypoint descriptor $V_p(n)$ which is shown as a 1D function (for a typical junction and non-junction) in Fig. 1. Since a cluster of responses in $V_p(n)$ correspond to only 1 vessel fragment, we locate the vessel edges by computing a first order difference of $V_p(n)$ as follows:
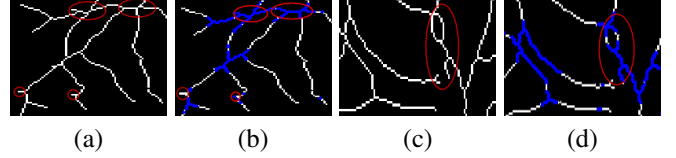
$$V_p'(n) = abs(V_p(n+1) - V_p(n)) \tag{1}$$
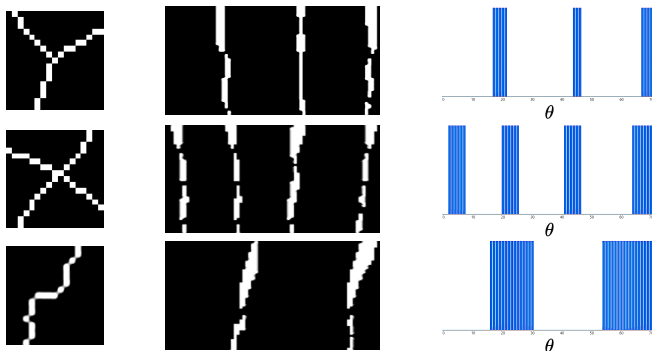
Fig. 1. Illustration of VKD. Column 1 (from top to bottom): sample bifurcation, crossover and a non-junction patch; Column 2: the corresponding Log-Polar maps (with x-axis being θ); Column 3: the final descriptor $V_p(n)$.

The number of vessel branches N at a point p is found as:

$$N(p) = \frac{1}{2} \sum_n V_p'(n) \tag{2}$$

We finally obtain a set of key points $C = \{p_i | N(p_i) > 2\}$.

Fig. 2. Challenges in keypoint detection. Red ellipses point to artefacts due to segmentation and skeletonization. (a),(c) Skeletonized vessel maps; (b),(d) Keypoints detected with VKD.

Figs. 2(a) and 2(c) show two challenging segmented vessel patches where complex vessel patterns can be seen. The detected keypoints are marked in blue in Figs. 2(b) and 2(d). These are seen mostly in the vicinity of junctions. A common type of artefact produced by segmentation are spurs appearing as a part of a vessel segment which lead to noisy keypoints. These are handled by setting $R_1 > k$ pixels with $k = 2$ or higher value. The effect of skeletonization also produces an artefact at vessel crossovers, namely a structure that resembles two closely placed bifurcations as depicted in Fig. 2(d). These are also tackled with a judicious choice of R_1 and R_2. It should be noted that since the vessel map is about 1 pixel thick, the parameters need to be fixed only once. We empirically found that $R_1 = 3px$, $R_2 = 8px$, $\Delta_r = 0.1$, $\Delta_\theta = 5°$ produce the best results. A sample sub-image, the corresponding thinned vessel map and detected keypoints are shown in Figs. 4(a) through 4(c).

3. A SYSTEM FOR JUNCTION DETECTION AND CLASSIFICATION

The proposed keypoint detector is used to design a system for vessel analysis. The input to this system is a skeletonised vessel map and output is a set of bifurcation and crossover points. The system design consists of the following steps: candidate junction selection, junction detection followed by classification. Details are presented next.

3.1. Junction candidates selection

Given a skeletonized vessel map, a set of keypoints are extracted using VKD as described in the above section. The obtained keypoints C appear as clusters of points close to junctions (as shown in Fig. 4(c)). These are refined to obtain the desired candidate junction points by noting that a junction point is where vessels of 2 or 3 different orientations meet. This can be characterised by the entropy of the histogram of

883

vessel orientations; points close to a junction will exhibit a higher entropy than those away [9]. For each point in C, a 3×3 neighborhood ω is considered and a Hessian matrix is computed for every pixel in ω and its second eigenvector is used to construct a curvature orientation histogram (COH) h_p. Finally, the entropy of COH $E(h_p)$ is obtained and a non-maximum suppression with a radius of 12 pixels is done to obtain the set of final candidate junctions C_j which are shown in Fig. 4(d).
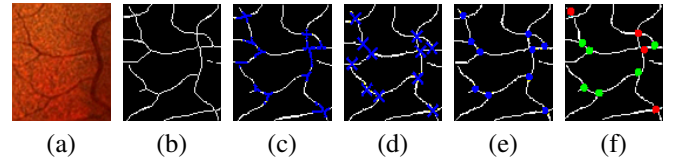
3.2. Junction detection

We propose a supervised learning technique for detecting true junctions. The VKD (V) and COH (h) features are extracted at every candidate points. These two features capture the vessel orientation information in a local neighborhood. Hence, they exhibit an excellent discriminative ability in distinguishing between a true junction J_n and a non-junction NJ_n. For each C_j, features are extracted from a 17×17 neighborhood and concatenated into a 1-D long vector $X_J = (V, h)$. A Random Forest (RF) classifier of 200 trees was trained. A sample result of the detected junctions is shown in Fig. 4(e).

3.3. Junction classification

Bifurcation versus crossover classification is a non-trivial task since it poses several challenges, which include ambiguity due to proximal presence of bifurcation and crossover points, multiple bifurcations/crossovers in a small region and parallel vessels. These are addressed by using a combination of features: orientation based (V, h) and shape based (response of basic Line Detector (LD) [10] and Histogram of Oriented Gradients (HOG) features. The LD (L) and HOG (O) primarily capture the local vessel shape information and can be used to accurately identify bifurcations and crossovers as shown in Fig. 3. For each detected true junction J_n, we compute (V, h, L, O) features in a 17×17 neighborhood. The line response at each pixel is obtained as explained in [10], which is vectorized to form a 1-D vector L. These features are concatenated to derive the final feature vector. A RF classifier with 500 trees is trained with these features to classify junctions J_n into bifurcations J_b and crossovers J_c. A sample result of the junction classification is shown in Fig. 4(f).

(a) (b) (c) (d) (e) (f)
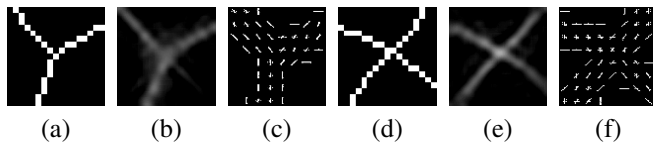
Fig. 3. Visualization of LD and HOG feature descriptors for sample bifurcation (a) and crossover (d) patches. (b), (e) and (c), (f) are the corresponding line response and the HOG map, respectively.

(a) (b) (c) (d) (e) (f)

Fig. 4. Junction detection and junction classification results. (a) A region of interest; (b) Skeletonized vessel map; (c) Result of VKD; (d) Candidate junctions; (e) Detected true junctions; (f) Identified bifurcations (green) and crossovers (red).

4. EXPERIMENTAL RESULTS

Experiments were done on five publicly available datasets. The details are provided in Table. 1. Ground truth (GT) labels for bifurcations and crossovers were derived for ARIA and CHASE_DB1 from two independent markers while for DRIVE, IOSTAR and STARE were shared by [5], [1]. As three independent markings exist for DRIVE [5], [1], [7], a majority consensus was taken to derive the GT. A half random split was done to generate the training and test sets from each dataset. The number of vessel junctions (bifurcations and crossovers) considered for evaluation is listed in Table. 1. The performance of the proposed approach was evaluated with the following metrics: sensitivity/recall (Se), specificity (Sp), accuracy (Acc), precision (Pr), F_1 score (F) and area under the ROC curve (AUC). Detected junctions within a radius of 4 pixels of GT points were taken to be true positives (TPs).

Table 1. Dataset split used in experiments. J_n denotes the number of junctions. Subscripts denote the type: bifurcations (b) and crossovers (c).

Dataset	Images	Training $J_n(J_b/J_c)$	Testing $J_n(J_b/J_c)$
DRIVE [11]	40	2684 (1923/761)	2064 (1513/551)
IOSTAR [1]	24	757 (550/207)	939 (663/276)
STARE [12]	20	2561 (1266/1295)	2489 (1291/1198)
CHASE_DB1 [13]	28	1575 (698/877)	1335 (580/755)
ARIA [14]	40	972 (682/290)	1168 (815/353)
Total	**152**	**8549**	**7995**

4.1. Junction detection results

A class imbalance exists between junctions and non-junctions classes in the set of candidates. This was handled with over-sampling by rotating the patches in arbitrary directions. A RF classifier of 200 trees was used for classification. The obtained values for different performance metrics are listed for the proposed method and the state-of-the-art method [1] in Table. 2. Our approach can be seen to outperform BICROS [1] on both DRIVE and IOSTAR, while it achieved the best

Se, Sp and F on all datasets. The higher Se is due to the discriminative power of VKD in differentiating vessel junctions from the complex background. The COHD is able to eliminate the false positives among the clusters of C leading to a higher Sp. Results reported by [4] on DRIVE and STARE are only on a subset of images precluding a thorough comparison. The GRAID method in [15] is evaluated using two different GT's on DRIVE whereas the data provided in [7] is the only one publicly available. Hence, we restrict our comparison to [7]. The results on CHASE_DB1 and ARIA data sets are also consistently high. Overall, the obtained results indicate that the proposed method is robust to changes in image resolution.

Table 2. Comparative evaluation of junction detection.

Method	Dataset	AUC	Acc	Se	Sp	Pr	F
BICROS	DRIVE	-	-	0.74	-	0.81	0.67
	IOSTAR	-	-	0.65	-	0.77	0.61
Our method	DRIVE	0.79	0.75	0.79	0.66	0.81	0.80
	IOSTAR	**0.90**	**0.85**	**0.87**	0.81	**0.94**	**0.90**
	STARE	0.83	0.78	0.80	0.73	0.89	0.85
	CHASE_DB1	**0.90**	0.81	0.80	**0.84**	0.93	0.86
	ARIA	0.79	0.71	0.70	0.74	0.87	0.78

Table 3. Comparative evaluation of junction classification.

Method	Dataset	AUC	Acc	Se	Sp	Pr	F
BICROS	DRIVE	-	0.83	0.59	0.91	-	-
	IOSTAR	-	0.83	0.67	**0.93**	-	-
Our method	DRIVE	0.93	0.87	0.86	0.87	0.70	0.77
	IOSTAR	**0.94**	0.89	**0.88**	0.89	0.76	0.82
	STARE	0.91	0.85	**0.88**	0.84	0.62	0.73
	CHASE_DB1	0.91	0.87	0.83	0.88	0.67	0.74
	ARIA	0.93	**0.90**	0.84	0.92	**0.81**	**0.83**

4.2. Junction classification results

Once again, a class imbalance is observed between the bifurcation and crossover classes which was handled by oversampling, by rotating the patches in arbitrary directions. An RF classifier with 500 trees was trained. Table. 3 depicts the bifurcation versus crossover classification performance. There is a boost in Se of $\approx 20\%$ relative to BICROS method. [7] reports only vessel bifurcation performance without taking into account the complex bifurcation/crossover structures. Similarly [4, 5] have reported the bifurcation/crossover classification performance independently against the background. Hence, the proposed approach cannot be directly compared with those methods. In general, most of the previous techniques are not able to model the complex bifurcation/crossover points whereas the proposed approach is able to better discriminate even a complex bifurcation/crossover points which have not been addressed previously in the literature. Hence, our method is more robust and reliable for junction classification task.

5. CONCLUSION

We have proposed a fully automatic, end-to-end solution for vessel keypoint analysis. This is based on a novel keypoint detector (VKD) which operates on a thinned vessel map and uses local orientation information to extract keypoints. The detected keypoints are in the vicinity of vessel junctions. The inclusion of shape information in addition to orientation aids in localizing junctions and classifying them accurately. Experimental results show the proposed system to be capable of handling the challenges posed by the thinning algorithms and robust to variations across datasets. It also outperforms state-of-the-art techniques on five publicly available retinal datasets. The proposed VKD has potential for extension to 3D and supporting further analysis of the vessel tree. These are some directions to be explored in the future.

6. REFERENCES

[1] Abbasi et al, "Automatic detection of vascular bifurcations and crossings in retinal images using orientation scores," in *ISBI*. IEEE, 2016, pp. 189–192.

[2] Habib et al, "The association between retinal vascular geometry changes and diabetic retinopathy and their role in prediction of progression–an exploratory study," *BMC ophthalmology*, vol. 14, no. 1, pp. 1, 2014.

[3] Hubbard et al, "Methods for evaluation of retinal microvascular abnormalities associated with hypertension/sclerosis in the atherosclerosis risk in communities study," *Ophthalmology*, vol. 106, no. 12, pp. 2269–2280, 1999.

[4] Aibinu et al, "Vascular intersection detection in retina fundus images using a new hybrid approach," *Computers in Biology and Medicine*, vol. 40, no. 1, pp. 81–89, 2010.

[5] Fathi et al, "Automatic vessel network features quantification using local vessel pattern operator," *Computers in biology and medicine*, vol. 43, no. 5, pp. 587–593, 2013.

[6] Favali et al, "Analysis of vessel connectivities in retinal images by cortically inspired spectral clustering," *Journal of Mathematical Imaging and Vision*, vol. 56, no. 1, pp. 158–172, 2016.

[7] Azzopardi et al, "Automatic detection of vascular bifurcations in segmented retinal images using trainable cosfire filters," *Pattern Recognition Letters*, vol. 34, no. 8, pp. 922–933, 2013.

[8] Su et al, "Junction detection for linear structures based on hessian, correlation and shape information," *Pattern Recognition*, vol. 45, no. 10, pp. 3695–3706, 2012.

[9] Ram et al, "Curvature orientation histograms for detection and matching of vascular landmarks in retinal images," in *SPIE Medical Imaging*. ISOP, 2009, pp. 72591J–72591J.

[10] Ricci et al, "Retinal blood vessel segmentation using line operators and support vector classification," *IEEE Trans on medical imaging*, vol. 26, no. 10, pp. 1357–1365, 2007.

[11] Staal et al, "Ridge-based vessel segmentation in color images of the retina," *IEEE Trans on medical imaging*, vol. 23, no. 4, pp. 501–509, 2004.

[12] Hoover et al, "Locating blood vessels in retinal images by piecewise threshold probing of a matched filter response," *IEEE Trans on Medical imaging*, vol. 19, no. 3, pp. 203–210, 2000.

[13] Fraz et al, "An ensemble classification-based approach applied to retinal blood vessel segmentation," *IEEE Trans on Biomed Engineering*, vol. 59, no. 9, pp. 2538–2548, 2012.

[14] "Aria online, retinal image archive," http://www.eyecharity.com/aria_online/, 2006.

[15] Núñez et al, "Growing algorithm for intersection detection (graid) in branching patterns," *Machine Vision and Applications*, vol. 26, no. 2-3, pp. 387–400, 2015.